



# Structural properties and failure characteristics of granite after thermal treatment and water cooling

Wenxi Li · Quangui Li · Yanan Qian ·  
Faping Ling · Ronghui Liu

Received: 20 January 2022 / Accepted: 26 November 2023  
© The Author(s) 2023

**Abstract** In a variety of fields such as exploitation of geothermal energy and the reconstruction of nuclear waste storage, both of high-temperature and cooling process change the physical and mechanical properties of granite. Uniaxial compression tests were performed on five groups of granite samples at 25 °C, 200 °C, 400 °C, 600 °C and 800 °C after water cooling, and CT scanning, acoustic emission(AE) monitoring and X-ray diffraction(XRD) scanning were used to investigate the structure properties and failure characteristics of granite. It is found that the proportions of pore volume greater than  $10^6 \mu\text{m}^3$  and less than  $10^5 \mu\text{m}^3$  with are positively and negatively correlated with the thermal treatment temperature respectively. The mechanical properties of granite are significantly deteriorated by temperature gradient shock, and crack development scale during failure process overall increases as implied by AE response. The failure intensity index  $\eta$  is proposed to characterize the failure severity of granite, and the value of  $\eta$  descends with the increase of thermal treatment temperature, indicating the failure severity of granite is alleviated.

Three types of loading failure mode are classified for water-cooled high-temperature granite. The failure mode of granite at 200 °C and 600 °C is tensile failure and tensile-shear failure respectively, while the granite samples are dominated by shear failure at 25 °C, 400 °C and 800 °C.

## Article Highlights

- Propose an index  $\eta$  to quantify the failure severity of granite.
- Higher temperature gradient alleviates the destructive effect of granite failure.
- The failure mode transfers from shear to tensile-shear as temperature gradient increases.
- The mechanism of irregular change of failure characteristics is analyzed.

**Keywords** High temperature · Granite · Water cooling · Pore structure · Mechanical properties · Failure characteristics

---

W. Li · Q. Li (✉) · Y. Qian · F. Ling · R. Liu  
State Key Laboratory of Coal Mine Disaster Dynamics  
and Control, Chongqing University, Chongqing 400044,  
China  
e-mail: liqq@cqu.edu.cn

W. Li · Q. Li · Y. Qian · F. Ling · R. Liu  
School of Resources and Safety Engineering, Chongqing  
University, Chongqing 400044, China

## 1 Introduction

The influence of high temperature on the engineering rock mass is of vital importance as the deep geotechnical engineering advances (Pathegama et al. 2017). Granite is widely distributed in the deep strata as a

common type of magmatic rock. Therefore, high-temperature granite suffers water cooling due to hydraulic fracturing, geothermal energy acquisition and other reasons in fields such as geothermal extraction, deep mineral extraction and nuclear waste repository construction (Shu et al. 2020; Watanabe et al. 2020; Zhang and Zhao 2020). Water cooling causes structural changes and increased damage to granite based on the effect of high-temperature. Hence, the study on structural properties and damage characteristics of high-temperature granite after water cooling is significant for deep geotechnical engineering.

The properties of high-temperature granites or naturally cooled granites after thermal treatment have been widely studied. Nasserli et al. (2007, 2009) systematically analyzed the evolution trend of permeability and fracture toughness in thermally treated Westerly granite. Chaki et al. (2008) investigated the changes of porosity and wave velocities of high-temperature granites. Shao et al. (2015) proved that thermal treatment prolongs the duration of stable crack propagation in granite by monitoring the AE response of failure process. And it was found that thermal treatment below 110 °C lead to negative damage in granite (Tian et al. 2021). The mechanism of thermal damage in granite at different high temperatures was studied by using X-ray micro CT, indicating that changes of strength and stiffness are closely related to the interactions of mineral particles (Yang et al. 2017). The thermal equilibrium state between mineral particles is broken due to different thermal stress. The weak rock bridges are destroyed when thermal stress exceeds the binding force between minerals, resulting in the generation of inter-granular cracks (Kumari et al. 2018b, a; Shen et al. 2021a, b). Because granite is a continuous material, the expansion and contraction of its internal particles are limited by each other. Therefore, thermal stress exists in the form of tensile stress on the rock surface and compressive stress in the interior (Kim et al. 2014). Under the action of thermal stress, cracks usually propagate along the path with the least energy consumption, and the areas with weak strength are damaged (Brotóns et al. 2013; Kumari et al. 2018b, a). When the thermal stress is strong enough to overcome the limitation of lattice energy, trans-granular cracks appear in the crystal (Jia et al. 2021).

Water cooling exacerbates the changes in the structural and mechanical properties of high-temperature

granites. Liu and Xu (2015) investigated the mechanical properties of high-temperature granite up to 600 °C after water cooling. The compressive strength, elastic modulus and ultrasonic wave velocity of the samples were found to decrease with increasing temperature. Kang et al. (2021) studied the mechanical properties of high-temperature granites after water cooling and analyzed the effect of mineral grain heterogeneity on the critical temperature. In terms of cooling conditions, the failure mechanism of high-temperature granite under different numbers of water cooling cycles was analyzed (Wu et al. 2022a, b). Research tools including X-Ray Scanning Diffraction (XRD) (Yin et al. 2021), Scanning Electron Microscopy (SEM) (Zhu et al. 2021a, b) and Optical Polarizing Microscopy (POL) (Junique et al. 2021) were applied to study the failure modes of high-temperature granite after water cooling. It was discovered that thermal shock lead to an increase in trans-granular cracks and a change in failure mode from tensile-shear failure to shear failure.

In general, the current research focuses more on the physical and mechanical properties of cooled granite after thermal treatment. However, the structural properties and failure characteristics of high-temperature granite after water cooling need to be systematically studied. In this study, uniaxial compression test was conducted on granite samples at 25 °C, 200 °C, 400 °C, 600 °C and 800 °C after water cooling. CT scanning test, XRD test and real-time monitoring of AE response were performed to study the changes in structural properties and failure characteristics of high-temperature granite after water cooling. The research results can provide reference for the safety of deep geotechnical engineering.

## 2 Materials and methods

### 2.1 Samples preparation

The granite studied is selected from Macheng City of Hubei Province, China. Rock mass of granite without apparent cracks or fissures was selected. Cylindrical samples of  $\Phi 50$  mm  $\times$  100 mm were drilled according to the requirements of the International Society of Rock Mechanics (ISRM). The flatness of the two ends of each sample was controlled within  $\pm 0.05$  mm, and deviation of the diameter within  $\pm 0.2$  mm, as

shown in Fig. 1. The P-wave velocity of each sample was measured after sample preparation. Samples with wave velocities ranging from 2700 to 2900 m/s were selected for subsequent processing to ensure the integrity of the samples.

### 2.2 Test process

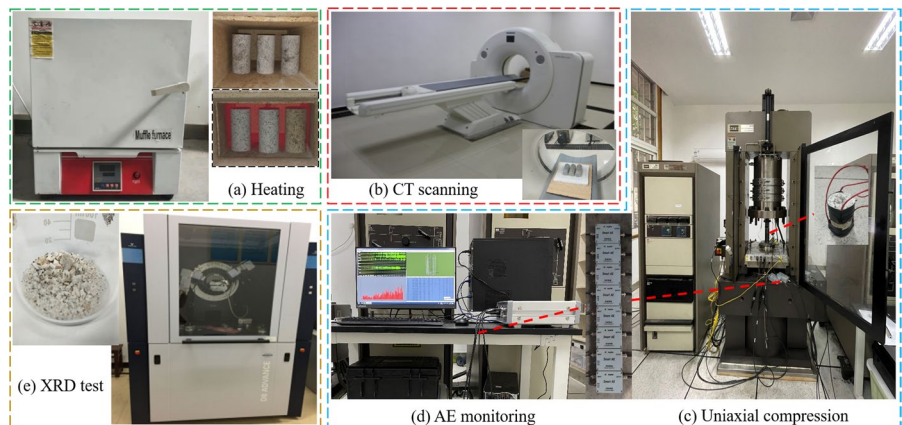
The samples were divided into five groups of A, B, C, D, E and numbered according to the preset

temperature levels. Samples of group A were kept at room temperature and calculated according to 25 °C. The remaining samples were heated to 200 °C, 400 °C, 600 °C and 800 °C, respectively. An electric box resistance furnace was used for thermal treatment. The heating rate was kept at 5 °C/min to moderate the effect of thermal shock (Zhu et al. 2021a, b). The samples were heated to the preset temperature and maintained in the furnace for 4 h. The samples during thermal treatment are shown in Fig. 2a. Then,



**Fig. 1** Geographic location of granite samples

**Fig. 2** Test equipment and process for structural and mechanical testing of granite after thermal treatment and water cooling



the samples were taken out and immersed into pure water at 25 °C. After water cooling, each sample was dried for 4h in drying oven. According to Fig. 2b, when all the samples were fully dried, CT scanning tests were performed on 5 groups of granite samples using the SOMATOM Ccope CT equipment with a resolution of 5.65  $\mu\text{m}$  and scanning layer thickness of 0.2 mm, which indicates that pores with size greater than 5.65  $\mu\text{m}$  can be effectively identified and counted.

As shown in Fig. 2c, the uniaxial compression tests were performed to all the samples by using MTS815 rock mechanics test system. With a loading rate of 0.1 mm/min, each sample was loaded to ultimate failure under displacement-control method. Additionally, assisted by a built-in displacement sensor, and the accuracy of each loading step reached 0.05%. The AE monitoring of each sample was monitored simultaneously with the DS5 AE monitoring system (Fig. 2d), while the signals were recorded by four resonant AE sensors (Model: RS-2A) as the preamplifier gain was 40 dB and sampling frequency was 4 MHz. The efficiency of each probe is guaranteed by a lead breakage test before the experiment. All the samples were collected after the uniaxial compression test, and the debris was grinded and sifted by a screen mesh (350 mesh) into powder samples. Subsequently, as shown in Fig. 2e, the XRD tests were conducted on powder samples with D8 ADVANCE X-ray diffractometer. The scanning mode was continuous scanning with the scanning speed of 3°/min, and the sampling interval was 0.02°.

### 3 Results

#### 3.1 Structural properties

The internal structure images of the samples are obtained by CT scanning. Different gray values in the images represent different material densities. Regions with the lowest gray value denote the pore. The threshold segmentation method is used to binarize the CT images, in order to quantitatively analyze the information of pore structure. Three-dimensional shape of sample is reconstructed, and the distribution of pore structure is shown in Fig. 3. The variation of the pore size distribution with the temperature gradient lays an important impact on the structural

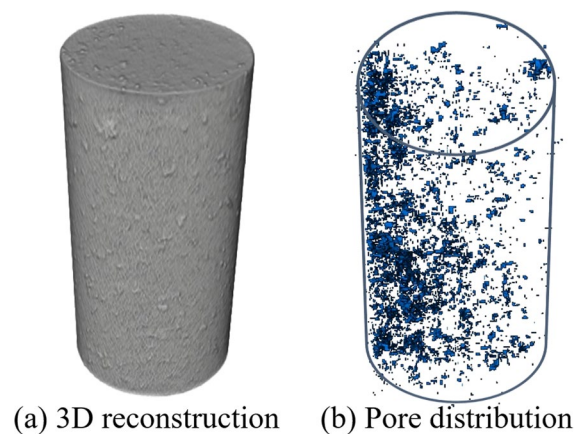


**Fig. 3** Schematic diagram for the pore structure of high-temperature and water-cooling treated granite sample

stability, especially considering the interaction of the pore size distribution with the fluid injection (Zhu et al. 2021a, b).

Figure 4 depicts the pore volume distribution and scanning slices of granite samples. These slices are the most porous of all the slices for each sample. Intuitively, the pore content in the slices increases with increasing thermal treatment temperature. Further, in order to quantify the pore size, the pore volume distribution of all samples with different thermal treatment temperatures is counted. It turns out that pore volumes of the untreated granite samples were all less than  $10^6 \mu\text{m}^3$ . When the temperature gradient increases, the percentage of pores with a volume greater than  $10^6 \mu\text{m}^3$  continues to increase and the pores smaller than  $10^5 \mu\text{m}^3$  gradually vanishes. At a thermal treatment temperature of 600 °C, the appearance of pores bigger than  $10^7 \mu\text{m}^3$  is observed. Eventually, the proportion of pores with a volume larger than  $10^8 \mu\text{m}^3$  is 7.3% at 800 °C, while that of pores smaller than  $10^5 \mu\text{m}^3$  is only 2.3%. The volume distribution of pores correlates well with temperature variation. This trend implies that the growth of heating temperature and temperature gradient complicate the pore structure.

The change in thermal treatment temperature also alters the mineral composition of granite, and consequently affect the structural properties of granite samples. In the XRD test, the direction and intensity of diffracted X-ray can characterize the diffraction features. Mineral composition of granite samples can

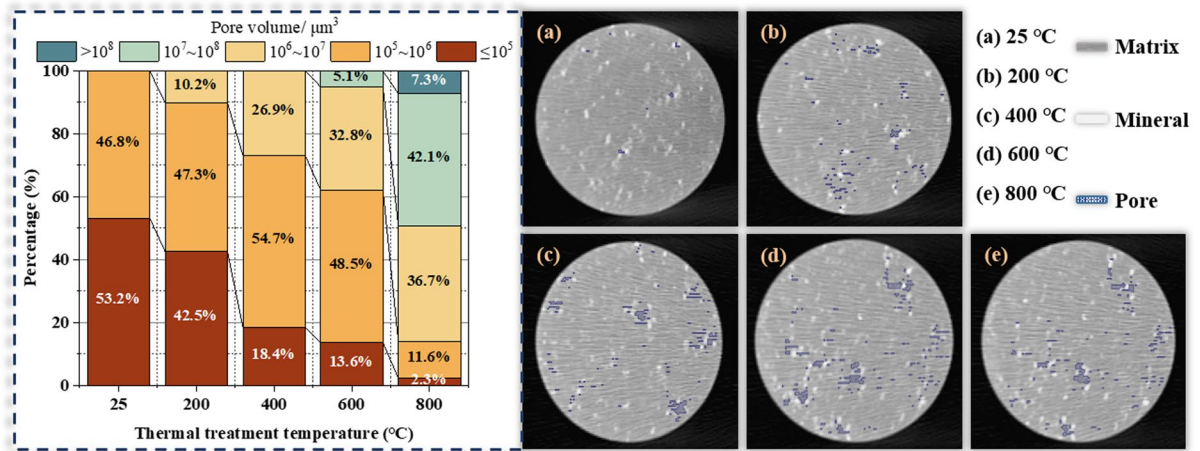


**Fig. 4** Pore volume distribution of granite samples after water cooling at different temperatures

be identified by X-ray diffraction spectrum. Relative content of each mineral component in granite samples at different temperatures after water cooling is calculated as:

$$W_X = \frac{I_X}{K_A^X \sum_{i=A}^N \frac{I_i}{K_A^i}} \quad (1)$$

where  $W_X$  is the relative content of a phase X, A is the name of the phase selected as the internal standard phase among the N phases,  $I_X$  is the diffraction intensity of phase X,  $K_A^X$  is the ratio of RIR value between phase X and internal standard phase A.

Main mineral compositions and their relative contents of high-temperature samples after water cooling are shown in Fig. 5 and Table 1. The granite used in this study is mainly composed of quartz, feldspar, and bits of mica and hornblende. The contents of quartz, mica and hornblende in granite samples increase continuously with the raise of thermal treatment temperature. The relative contents of quartz, mica and hornblende increase from 23.8%, 12.1% and 2.2% at 25 °C to 25.8%, 13.1% and 3.5% at 800 °C, respectively. On the contrary, the content of feldspar descends with the increase of thermal treatment temperature, and finally decreases from 61.9% at 25 °C to 57.6% at 800 °C.

In Fig. 5, when the thermal treatment temperature reaches 600 °C, the diffraction intensity of feldspar increases significantly with a bimodal phenomenon in

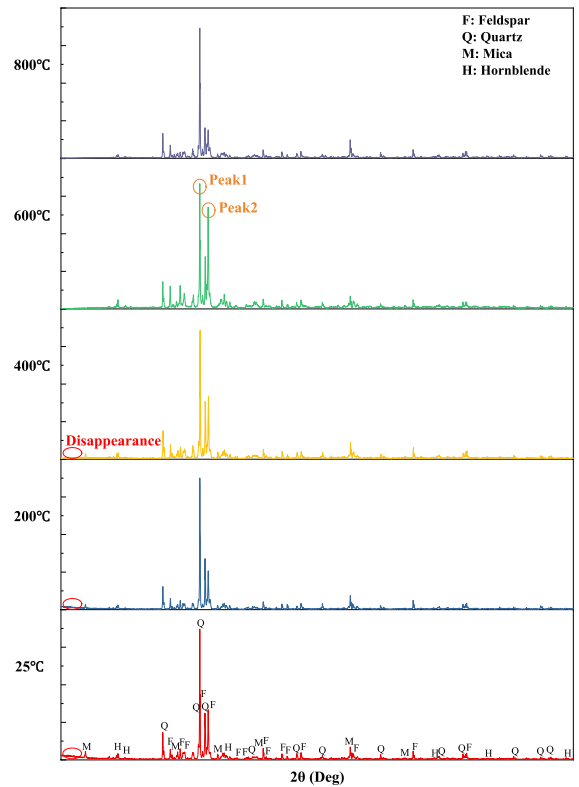


**Fig. 5** X-ray diffraction (XRD) spectrum of granite after water cooling at different heating temperatures

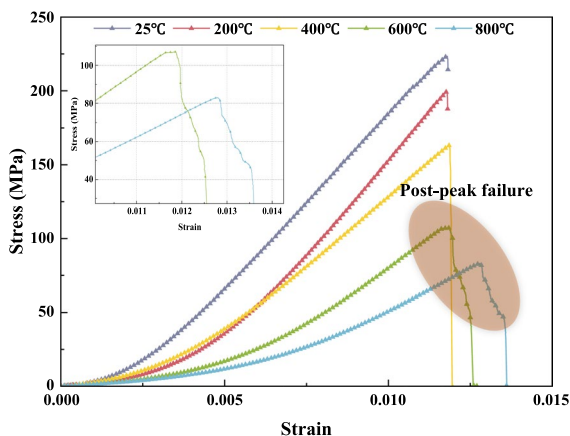
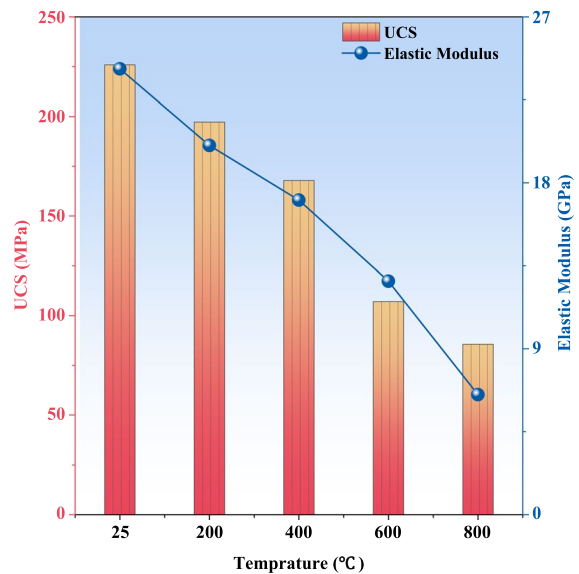
**Table 1** Relative contents of the main mineral components at different temperatures (unit: %)

Temperature (°C)	Feldspar	Quartz	Mica	Hornblende
25	61.9	23.8	12.1	2.2
200	61.1	24.3	12.4	2.2
400	60.4	24.5	12.7	2.4
600	58.2	25.4	13.5	2.9
800	57.6	25.8	13.1	3.5

the diffraction spectrum. Moreover, the spikes of low diffraction intensity are reduced when the temperature is above 200 °C. The results imply that the mineral impurities decrease with the rise of thermal treatment temperature, and the effect of mineral impurities on main minerals is gradually weakened.

### 3.2 Mechanical properties and AE characteristics

The stress–strain curves of uniaxial compression failure of granite samples are shown in Fig. 6. The uniaxial compressive strength (UCS) of granite samples descends with the increase of thermal treatment temperature, and the peak strain surges at 400 °C, 600 °C and 800 °C. The stress–strain curves of granite after water cooling at 600 °C and 800 °C show an obvious post peak stage with the characteristics of plastic failure.

**Fig. 6** Stress–strain curves of granite after water cooling at different temperatures**Fig. 7** Variation of strength and elastic modulus of granite after water cooling at different temperatures

The average values of UCS and elastic modulus of each group of samples are calculated, and the results are shown in Fig. 7. The value of UCS and that of elastic modulus are 225.88 MPa and 24.18 GPa when the samples are at 25 °C. After being heated to 200 °C, 400 °C, 600 °C and 800 °C, the UCS of each group of samples after water cooling is 197.25 MPa, 167.83 MPa, 107.08 MPa and 85.60 MPa, respectively. The elastic modulus also decreases with the growth of thermal treatment temperature. The average elastic modulus at 200 °C, 400 °C, 600 °C and 800 °C is 20.03 GPa, 17.06 GPa, 12.67 GPa and 6.51 GPa, respectively. The elastic modulus at 800 °C is 73.08% lower than that at 25 °C, indicating that the mechanical properties of granite are seriously deteriorated under thermal treatment and water cooling (Wu et al. 2022a, b).

In order to further study the failure response of each sample, the temporal distributions of AE ring counts and accumulated AE counts of different samples are shown in Fig. 8. The value of AE ring counts reflects the activity of internal damage and defect of rock. A higher number of AE ring counts correspond to the increase of crack number and the degree of fracture development.

During uniaxial compression, the temporal distribution of AE ring counts of each sample is consist

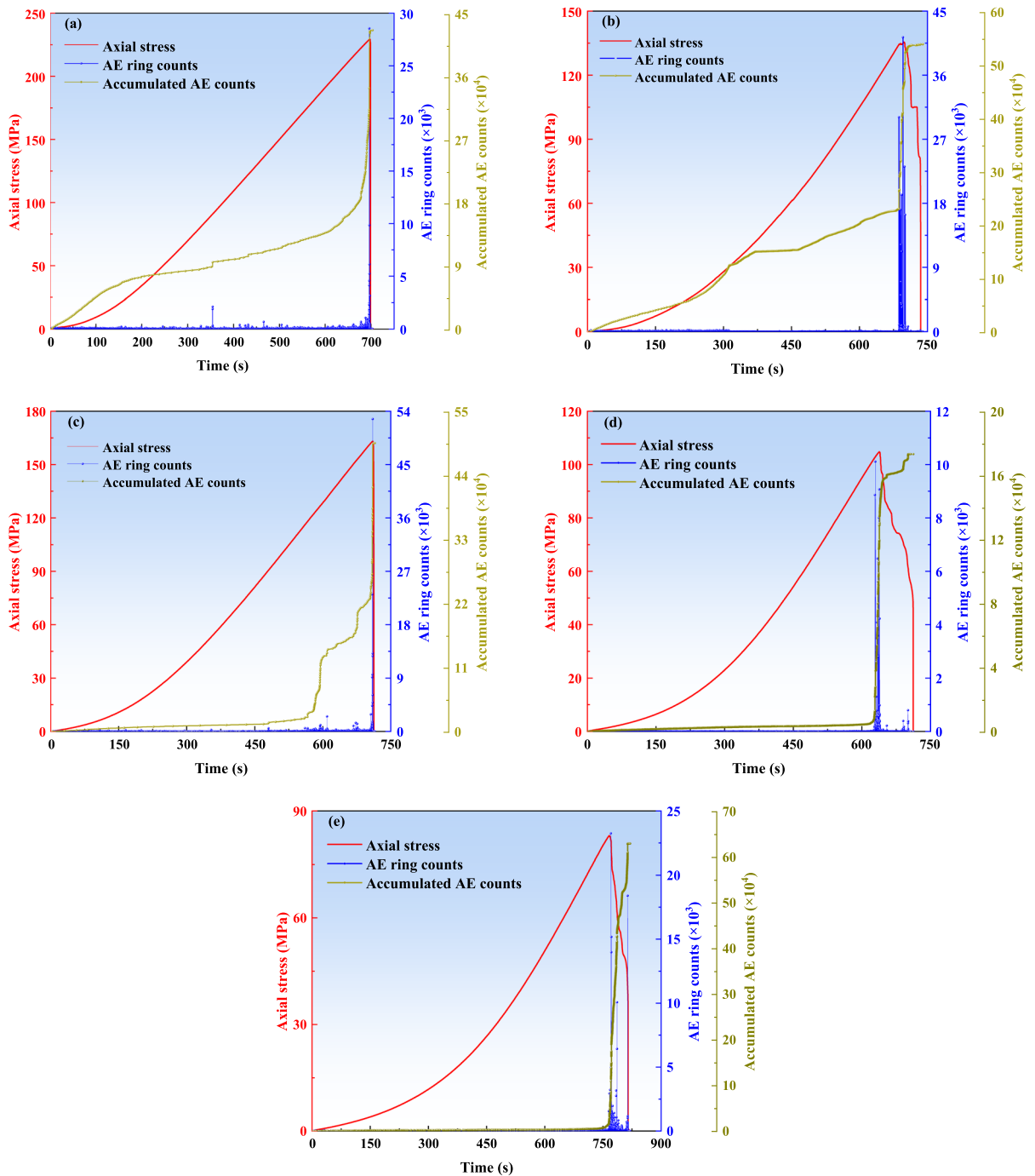


**Fig. 8** Stress–strain and AE curves of granite under uniaxial compression test at high temperatures. **a** T=25 °C, **b** T=200 °C, **c** T=400 °C, **d** T=600 °C, **e** T=800 °C

with the stress evolution trend. In Fig. 8d, e, the curve of accumulated AE counts is relatively flat during the compacting stage, since the development of internal

cracks is sufficient due to thermal treatment and water cooling before loading. During the elastic stage, the degree of fracture development decreases, and the

value of AE ring counts is low. In the plastic deformation stage, the connection of fractures and pores leads to the rise of AE ring counts. The internal cracks of sample continue to expand and produce the main fracture at the failure stage. The value of AE ring counts soars, and the maximum value appears near the peak strength. In addition, the granite samples change from brittle to ductile failure when the thermal treatment temperature reaches 600 °C. Consequently, as shown in Fig. 8d, e, the samples also experience a distinct post-peak damage process after the peak stress, and a series of acoustic emission signals can be observed during this period.

As shown in Fig. 9, the peak ring counts and accumulated ring counts of each sample own a similar evolution trend with the variation of thermal treatment temperature. In terms of peak ring counts, the value at 200 °C and 400 °C increases by 290.29% and 184.46% respectively compared with that at 25 °C. Nevertheless, the value of peak ringing counts drops at 600 °C and 800 °C, which is 64.60% and 18.60% lower than that at 25 °C respectively. The reason for the decrease of peak ringing counts is the reduction of energy release when the main fracture occurs, which indicates that the fracture development is distinctly promoted by thermal treatment and water cooling at 600 °C and 800 °C.

Significantly, a certain difference between the peak ring counts and accumulated ring counts exists when thermal treatment temperature is 800 °C. The value of accumulated ring counts increases sharply to the maximum at 800 °C. This change accords with the large failure scale and an obvious post peak failure stage at 800 °C. Moreover, after thermal treatment and water cooling, the value of accumulated ring counts of granite generally increases compared with that at 25 °C, which manifests that the crack number and failure scale are enlarged in the failure process.

### 3.3 Energy evolution and failure severity characteristics

According to Xie et al. (2005), rock deformation and fracture is the comprehensive result of energy release and dissipation. It is assumed that the heat exchange between rock mass elements and the external environment is avoided. According to the first law of thermodynamics, the total energy  $U$  generated by external force is:

$$U = U_e + U_d = U_1 = \int \sigma_1 d\epsilon_1 \quad (2)$$

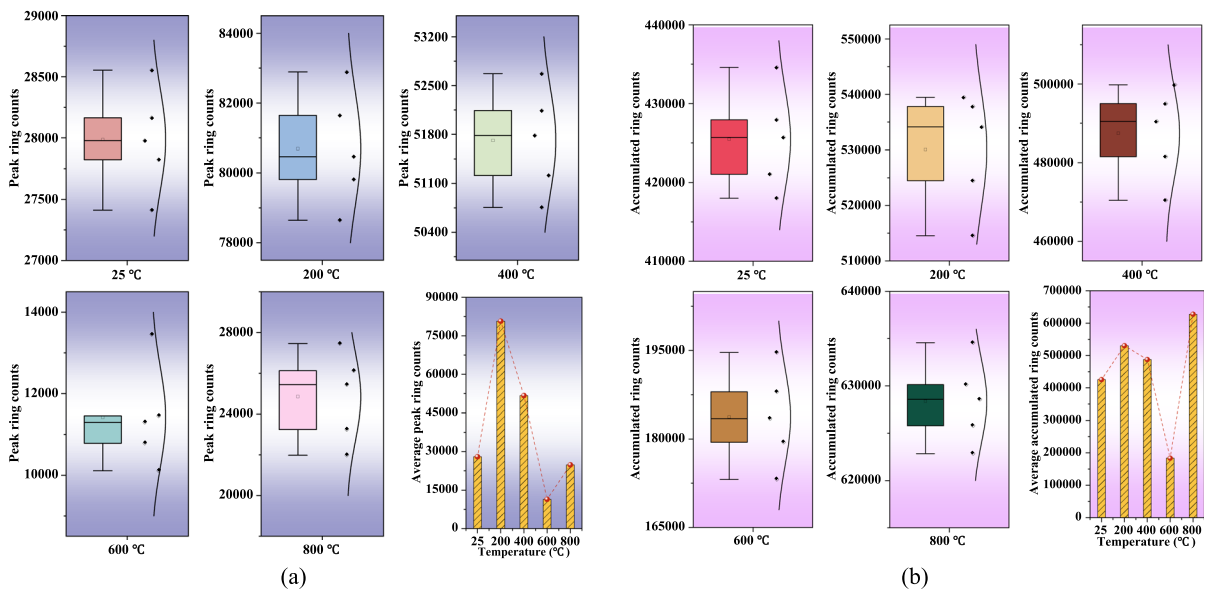


**Fig. 9** Characteristic parameter values and mean distribution of samples at different heating temperatures. **a** Peak ring counts; **b** accumulated ring counts



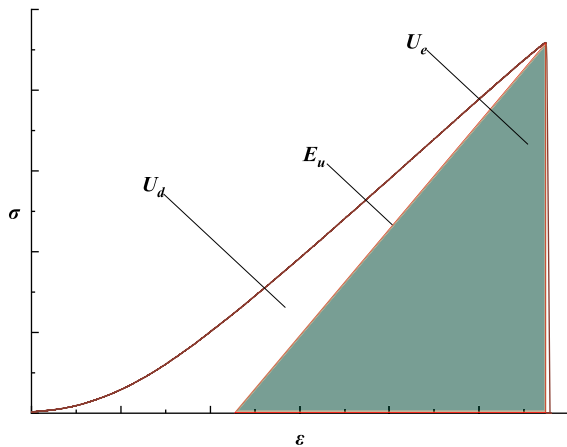


**Fig. 10** Relationship between dissipated strain energy and releasable strain energy in stress–strain curve

where  $U_e$  is the releasable strain energy ( $\text{MJ m}^{-3}$ ),  $U_d$  is dissipated energy ( $\text{MJ m}^{-3}$ ),  $U_l$  is the strain energy density generated by axial force ( $\text{MJ m}^{-3}$ ),  $\sigma_1$  is axial stress (MPa),  $\varepsilon_1$  is axial strain.

The connection between  $U_e$  and  $U_d$  is illustrated in Fig. 10. The colored area denotes the releasable strain energy  $U_e$ . The development of damage in sample is accompanied by energy dissipation, while part of total energy is stored in the form of  $U_e$ . When the  $U_e$  exceeds the surface energy of mineral particles, the rock element will be destroyed. Under uniaxial compression, the releasable strain energy  $U_e$  is calculated as:

$$U_e = \frac{\sigma_1^2}{2E_u} \tag{3}$$

and the dissipated energy is  $U_d$ :

$$U_d = \int_0^{\varepsilon_1} \sigma_1 d\varepsilon_1 - \frac{\sigma_1^2}{2E_u} \tag{4}$$

The energy evolution trend of each sample during uniaxial compression test is calculated, and the result is shown in Fig. 11. As shown in Fig. 11c, e, sudden decrease of  $U_e$  happens in the plastic deformation stage, which denotes a certain scale of damage in the sample. Consequently, the released elastic waves are detected by AE sensors. According to Fig. 8, the number of AE ring counts increases

significantly in the plastic deformation stage, and it proves that AE response of failure process consists with the energy evolution characteristics. With the further increase of loading, the sample cannot support the continuous aggregation of  $U_e$ . Therefore, a large-scale release of  $U_e$  occurs. The internal structure of sample is deteriorated and the strength is reduced.

Table 2 shows the energy of different samples when loaded at UCS. As the thermal treatment temperature grows, the value of total energy  $U$  descends obviously, while an overall reduction of the dissipated strain energy and releasable strain energy at UCS also exists. For samples that heated to 800 °C, the value of  $U_e'$  is greater than that at 600 °C. The reason is that the surface energy of mineral particles rises, and the ability to store the releasable strain energy is enhanced.

In order to further analyze the failure characteristics of granite samples, the failure intensity is studied from the perspective of energy evolution. Under the assumption that the total energy  $U$  remains constant at UCS, the greater the difference between  $U_e$  and  $U_d$ , the less damage of sample and the stronger energy could be released when the rock is broken. In this situation, the energy released is greater when rock failure happens, and the failure intensity and scale of damage area increase. Therefore, the failure intensity index  $\eta$  is proposed to characterize the severity of rock failure. The failure intensity index  $\eta$  is calculated as:

$$\eta = \frac{U_e' - U_d'}{U'} \tag{5}$$

The variation of failure intensity index  $\eta$  is shown in .

Table 2 the value of  $\eta$  at a thermal treatment temperature of 200 °C, 400 °C, 600 °C and 800 °C drops by 11.53%, 21.77%, 27.43% and 22.95% respectively compared with that at 25 °C. The value of  $\eta$  owns a downward trend when thermal treatment temperature ascends, though the value of  $\eta$  at 800 °C is greater than the value at 600 °C. The decline of the value of  $\eta$  illustrates that the failure severity of granite is mitigated with the increase of thermal treatment temperature. Generally, the failure severity of granite is alleviated by thermal treatment and water cooling.

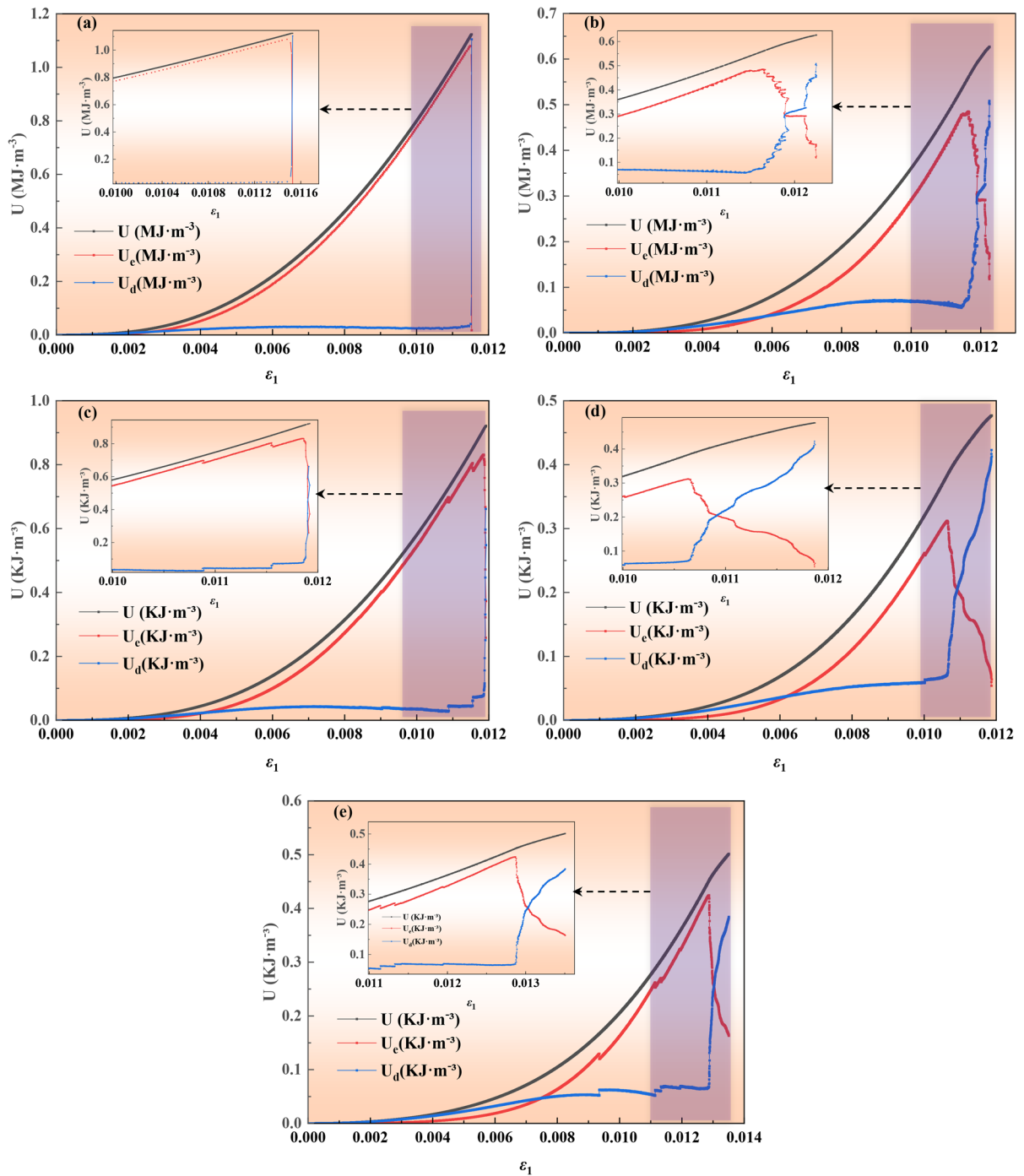


**Fig. 11** Curves of energy evolution of granite after water cooling at different temperatures. **a**  $T = 25^\circ\text{C}$ , **b**  $T = 200^\circ\text{C}$ , **c**  $T = 400^\circ\text{C}$ , **d**  $T = 600^\circ\text{C}$ , **e**  $T = 800^\circ\text{C}$

**Table 2** Energy and index of failure intensity of granite after water cooling at UCS

T (°C)	$U'$ (Kj m <sup>-3</sup> )	$U_e'$ (Kj m <sup>-3</sup> )	$U_d'$ (Kj m <sup>-3</sup> )	$\eta$
25	1116.17	1080.72	35.45	0.94
200	909.14	831.37	77.77	0.83
400	559.95	485.29	74.66	0.73
600	383.64	322.17	61.47	0.68
800	451.71	388.99	62.72	0.72

$U'$ : total energy at UCS;  $U_e'$ : releasable strain energy at the value of UCS;  $U_d'$ : dissipated energy at the value of UCS

### 3.4 Micro-cracks evolution trend

Rock failure is caused by the combined action of tensile crack and shear crack. Tensile crack is characterized by high frequency and short rise time, while the frequency of shear crack is relatively lower and the rise time is longer. Accordingly, Ohno and Ohtsu (2010) proposed a method to judge the fracture type by  $RA$  value and  $AF$  value. For one AE event, the value of  $RA$  equals to the specific value of the rise time to maximum amplitude, and  $AF$  equals to the ratio of AE ringdown-count to the duration time.

As shown in Fig. 12a, for untreated samples, the  $RA$  values are lower in Stage I (compaction stage), where crack initiation is rare and the type of tensile crack is dominant. As the temperature gradient increases, the  $RA$  values begin to grow due to the appearance of shear cracks within Stage I. The  $RA$  values increase as the temperature gradient increases. At Stage II (elastic deformation stage), the  $AF$  values of different samples exhibit an overall decreasing trend, while the  $RA$  values present similar change characteristics. This stage is mainly accompanied by mixed tension-shear cracks. Moreover, when the  $RA$  value increases with increasing thermal treatment temperature, it could be inferred that the granite samples are more inclined to generate shear cracks within Stage II after the temperature gradient shock. Subsequently, the  $RA$  values grow gradually in stage III (unstable crack development stage), accompanied by unstable fluctuations in the  $AF$  values, indicating that both tensile and shear cracks are formed in large quantities, and that mixed tensile-shear cracks exist. Eventually, at stage IV (failure stage), the  $RA$  values surge as the thermal treatment temperature increases, in conjunction with increasing  $AF$  values. It can be assumed that a large number of large-scale shear

cracks develop through the stage IV, and the thermal shock leads to the sample in the failure process is more likely to form shear fractures. These fractures, together with shear cracks and mixed tensile-shear cracks, lead to the ultimate failure.

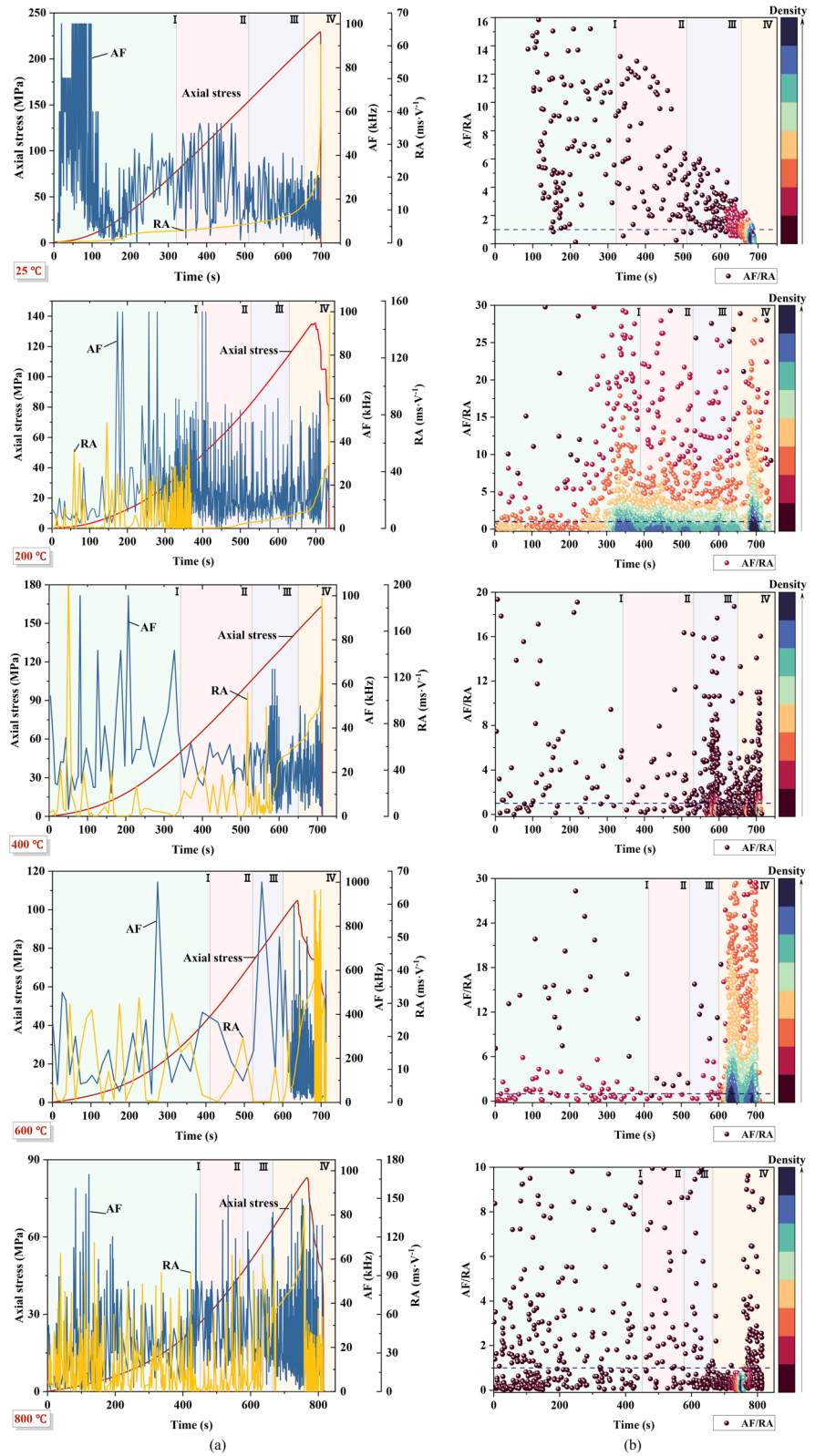
In order to reflect the temporal evolution trend of crack type more intuitively, the point density diagram of  $AF/RA$ -time is depicted in Fig. 12. The greater the density of a point, the more significant its effect on the failure of granite. Besides, the ratio of  $AF$  (kHz) to  $RA$  (ms/V) is utilized to illustrate the crack types, and a reference line of  $AF/RA=1$  is also applied. Data points are distributed on both sides of the reference line, which manifests that both of tensile crack and shear crack are engaged in the failure of different samples.

Significantly, as shown in Fig. 12b, for samples that treated to 600 °C, the nucleation region of density map extends from the area of shear crack to that of tensile crack, indicating that both shear crack and tensile crack are critical for rock failure. However, the nucleation region concentrates at the area of tensile crack at 200 °C, and mainly aggregates at the area of shear crack at other temperatures. Accordingly, three types of failure mode of granite exist at different thermal treatment temperatures. The failure mode of granite at 25 °C, 400 °C and 800 °C is shear failure, while tensile failure and tensile-shear failure is dominant at 200 °C and 600 °C respectively. For the same sample, micro-cracks exhibit a trend of transforming from tensile cracks to shear cracks during the loading process, especially in stage IV where micro-cracks are mainly concentrated in the area of shear cracks.

## 4 Discussion

In this study, granite samples were subjected to high temperature heating followed by water cooling. In order to analyze how the pore structure and chemical composition of granite are affected by changes in temperature, CT scanning and XRD tests were conducted. Uniaxial compression experiments were carried out on samples that under different treatment conditions, and the whole process of AE monitoring was performed at the same time. It turns out that the pore volume of granite is more diffuse with increasing temperature gradient, and the mineral composition is significantly changed. Meanwhile, the energy

**Fig. 12** Temporal evolution of micro-cracks classification for high-temperature granite under uniaxial compression test after water cooling. **a** Stage characteristics of RA-AF value; **b** AF/RA density distribution



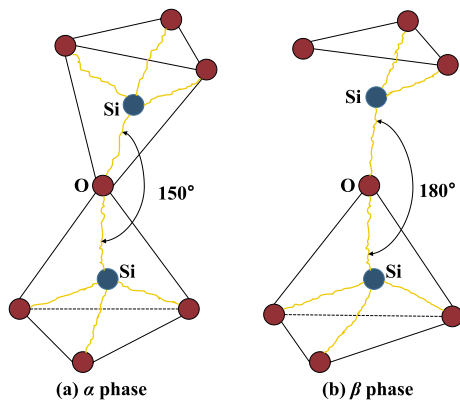


**Fig. 13** Change in the quartz bond angle from  $\alpha$  phase (a) to  $\beta$  phase (b)

evolution and mechanical properties of granite are found to change critically at 600 °C. In particular, the AE response exhibits an irregular correlation with the temperature gradient. In addition, the samples are destabilized at a thermal treatment temperature of 600 °C in the most intense scale, evaluated by the failure intensity index  $\eta$ .

The results accord with the finding that the quartz transforms from  $\alpha$  phase to  $\beta$  phase at 573 °C (Hartlieb et al. 2016; Ohno 1995). As shown in Fig. 13, the angle between two different Si–O tetrahedrons changes from 150° to 180° in quartz lattice. Phase transformation of quartz is accompanied by volume expansion and drop of crystal energy (Shen et al. 2021a, b; Smalley and Marković 2019). Thus, as shown in Fig. 11, the value of releasable strain energy varies with the change of temperature. When the temperature of granite reaches between 600 and 800 °C, the brittle components of granite transforms to plastic materials (Sun et al. 2015). In general, physical and chemical changes are generated in granite under the effect of thermal treatment. Chemical changes occur when the temperature is relatively high, and physical transitions exist in the whole process.

According to Sect. 3.4, when high-temperature granite is cooled by water, the proportion of shear cracks in the uniaxial compression failure process of the sample gradually increases with the expansion of temperature gradient. This result can be attributed to the distribution of pores and cracks caused by high temperature and thermal stress. As shown in Fig. 14, during the thermal treatment and water cooling processes, changes in the structure of

mineral particles and cracks generated by mechanical actions form shear planes inside the sample, leading to the continuous formation of shear cracks at the tip of the plane during loading. But interestingly, when the granite has not been heated to 600 °C, the macroscopic failure mode is closer to shear failure, and the cracks penetrate diagonally through the entire sample. When heated to 600 °C and 800 °C, tensile cracks distributed in the axial direction are observed, indicating a certain difference between the proportion of micro-cracks and the macroscopic failure morphology. The proportion of different cracks is quantitatively analyzed based on the criteria proposed by Dong et al. (2023). A baseline of  $AF = 11RA(10^5 \mu\text{s/V}) + 60$  is applied to classify the crack type. The proportion of shear crack accounts for 45.6% at the temperature of 25 °C, and the proportion of shear crack in failure process is 55.9%, 53.4% and 48.4% respectively at 200 °C, 400 °C and 600 °C. Differently, the proportion of shear crack surges to 70% at the thermal treatment temperature of 800 °C. This indicates that the temperature affects the proportion of rock micro-cracks, which leads to the discrepancy in the macro-failure modes.

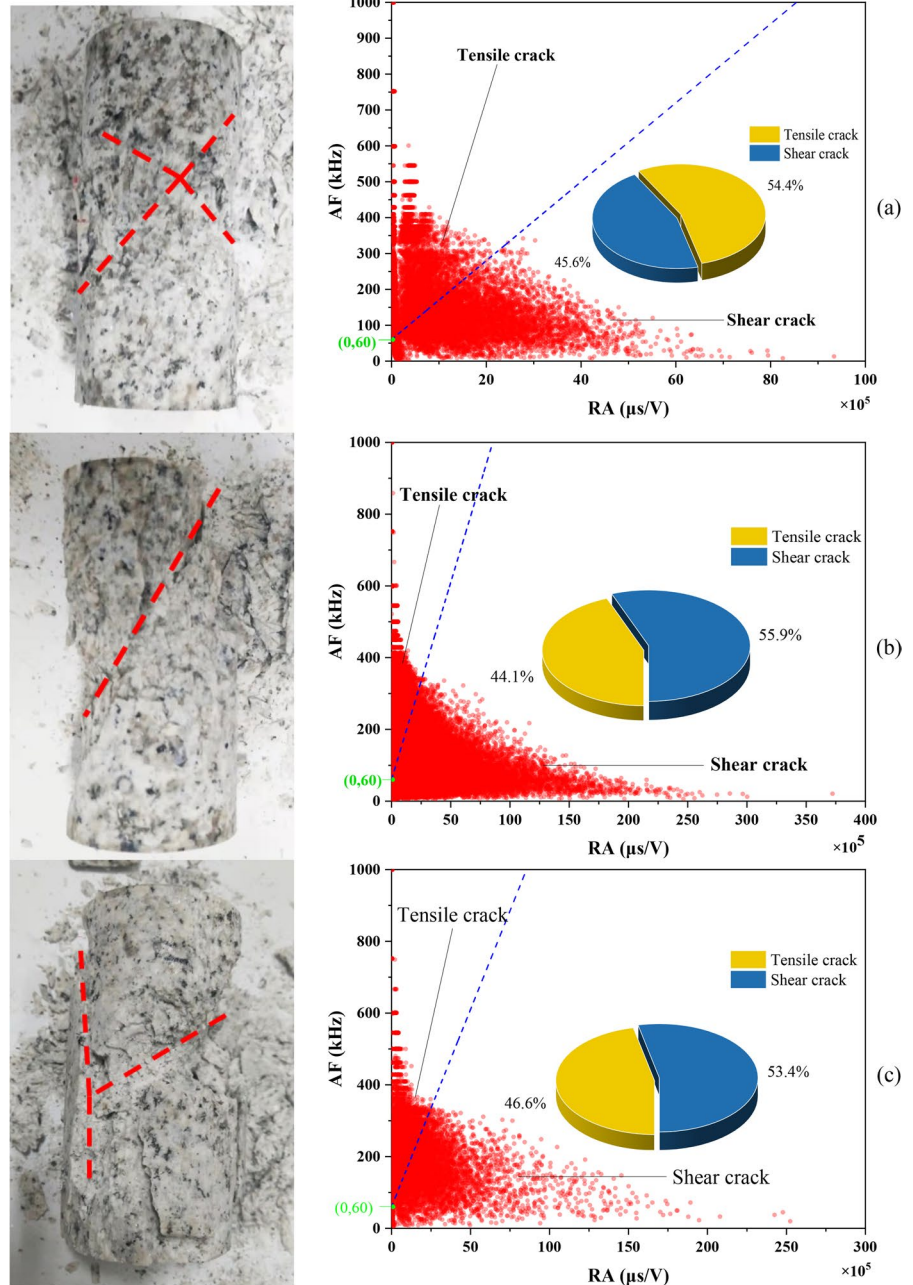
Additionally, the movements of mineral particles in granite under thermal treatment and water cooling are shown in Fig. 15. After thermal treatment and thermal insulation treatment, the interior of the rock is approximately in thermal equilibrium. When the sample is put into cooling water, sudden change of thermal stress is caused by thermal shock, and the thermal stress is:

$$\sigma_{ts} = E\Delta\alpha\Delta T \quad (6)$$

where  $E$  is the elastic modulus of sample,  $\Delta\alpha$  is the variation of thermal expansion coefficient,  $\Delta T$  is the difference of temperature. The irregular change of failure characteristics of granite may due to the competition between thermal hardening and damage (Heap et al. 2017; Meredith and Atkinson 1985), and the competition affects the failure characteristics in terms of structural properties and strength of granite.

The irregular change of failure characteristics is also related to the anisotropy of granite. Water cooling generally intensifies the formation of cracks in granite, but the strong temperature gradient may lead to the growth of non-uniform plastic strain

**Fig. 14** Morphology of sample failure and statistical charts of micro-cracks classification for high-temperature granite under uniaxial compression test after water cooling. **a**  $T=25\text{ }^{\circ}\text{C}$ , **b**  $T=200\text{ }^{\circ}\text{C}$ , **c**  $T=400\text{ }^{\circ}\text{C}$ , **d**  $T=600\text{ }^{\circ}\text{C}$ , **e**  $T=800\text{ }^{\circ}\text{C}$



field and material hardening (Zhang et al. 2018). The water cooling treatment can lead to the solidification of fluids in the high-temperature granite, resulting in the increase of rigidity in limited area. The orientation and shape of fractures are also complicated. Consequently, under the effects of thermal treatment temperature and water cooling, the irregular change of failure characteristics such

as AE response and failure mode of granite occur. Moreover, as the temperature gradient increases during sample processing, more trans-granular cracks are generated as a result of water-cooling shocks. Consequently, the induced intergranular and trans-granular cracks prompt the failure modes of granite samples change from tensile failure to shear dominant failure, hence the tensile-shear failure is

Fig. 14 (continued)

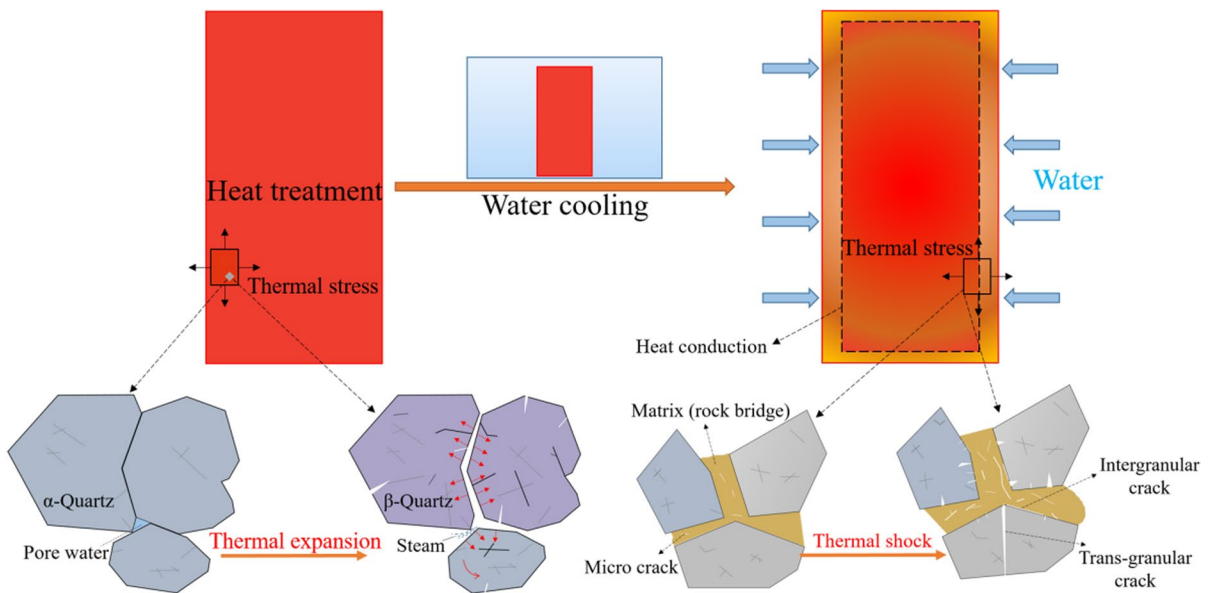
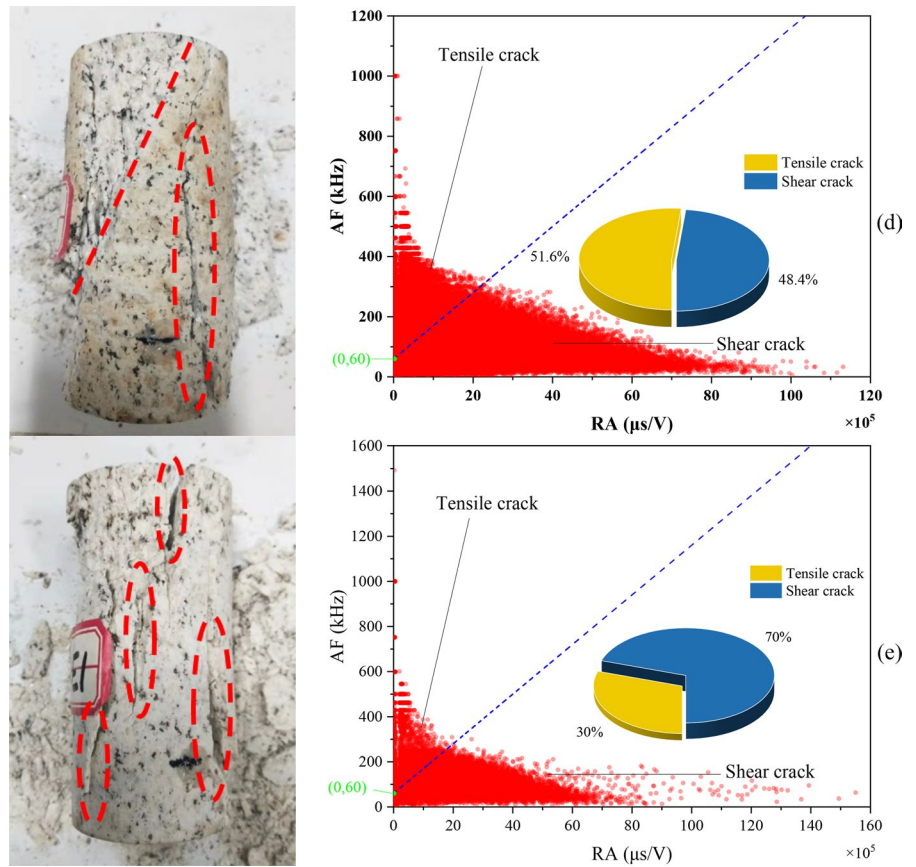


Fig. 15 Microstructure development process of high-temperature granite subjected to water cooling

also observed with the increasing thermal treatment temperature.

In fact, one limitation of this research was that due to thermal radiation and heat conduction, the actual temperature of granite during thermal treatment surpassed the preset temperature. However, from the results of each sample, the trend in structural properties and failure response of granite after thermal treatment and water cooling emerged, which aids to appreciate the geo-mechanical evaluation in field with fluids injection.

## 5 Conclusions

Pore structure and mineral components of granite samples determine the physical response under loading. The pore structure of granite is complicated by thermal treatment and water cooling. As the temperature gradient ascends, the percentage of pores that bigger than  $10^6 \mu\text{m}^3$  continues to increase while that of pores smaller than  $10^5 \mu\text{m}^3$  decreases. The feldspar composition of granite reduces after heating, while the content of quartz increases. Under uniaxial compression, the elastic modulus and UCS of granite drop when the samples are heated to a higher temperature and cooled by water. In addition, the value of accumulated AE counts overall increases at a higher temperature, indicating the increase of crack development scale during failure process.

Energy evolution can account the essence of rock failure, the failure intensity index  $\eta$  is proposed to characterize the destructive effect of rock failure. The value of  $\eta$  descends when the thermal treatment temperature rises. The decrease of  $\eta$  manifests that the destructiveness of failure of granite is weakened by thermal treatment and water cooling, while it turns out that the failure intensity approaches the highest when heated to 600 °C. By contrast, in terms of failure characteristics, failure modes of granite samples are prone to be complicated. During the loading process, the type of micro-cracks shifts from tensile cracks to shear cracks. The failure modes of high-temperature granite cooled by water are classified into shear failure, tensile failure and tensile-shear failure. The shear failure is predominant at 25 °C, 400 °C

and 800 °C, and the failure mode of granite at 200 °C and 600 °C is tensile failure and tensile-shear failure, respectively. This study may render a reference for assessing failure characteristics of high-temperature granite and evaluating its stability with fluid injection.

**Acknowledgements** This research was supported by the National Natural Science Foundation of China (Grant No. 52074049).

## Declarations

**Competing interest** The authors declare that they have no known competing financial interests or personal relationships that could have appeared to influence the work reported in this paper.

**Open Access** This article is licensed under a Creative Commons Attribution 4.0 International License, which permits use, sharing, adaptation, distribution and reproduction in any medium or format, as long as you give appropriate credit to the original author(s) and the source, provide a link to the Creative Commons licence, and indicate if changes were made. The images or other third party material in this article are included in the article's Creative Commons licence, unless indicated otherwise in a credit line to the material. If material is not included in the article's Creative Commons licence and your intended use is not permitted by statutory regulation or exceeds the permitted use, you will need to obtain permission directly from the copyright holder. To view a copy of this licence, visit <http://creativecommons.org/licenses/by/4.0/>.

## References

- Brotóns V, Tomás R, Ivorra S, Alarcón JC (2013) Temperature influence on the physical and mechanical properties of a porous rock: San Julian's calcarenite. *Eng Geol* 167:117–127. <https://doi.org/10.1016/j.enggeo.2013.10.012>
- Chaki S, Takarli M, Agbodjan WP (2008) Influence of thermal damage on physical properties of a granite rock: porosity, permeability and ultrasonic wave evolutions. *Constr Build Mater* 22(7):1456–1461. <https://doi.org/10.1016/j.conbuilmat.2007.04.002>
- Dong L, Zhang Y, Bi S, Ma J, Yan Yihao, Cao Heng (2023) Uncertainty investigation for the classification of rock micro-fracture types using acoustic emission parameters. *Int J Rock Mech Min* 162:105292. <https://doi.org/10.1016/j.ijrmms.2022.105292>
- Hartlieb P, Toifl M, Kuchar F, Meisels R, Antretter T (2016) Thermo-physical properties of selected hard rocks and their relation to microwave-assisted comminution. *Miner Eng* 91:34–41. <https://doi.org/10.1016/j.mineng.2015.11.008>



- Heap MJ, Violay M, Wadsworth FB, Vasseur J (2017) From rock to magma and back again: the evolution of temperature and deformation mechanism in conduit margin zones. *Earth Planet Sci Lett* 463:92–100. <https://doi.org/10.1016/j.epsl.2017.01.021>
- Jia P, Yang Q, Liu D, Wang S, Zhao Y (2021) Physical and mechanical properties and related microscopic characteristics of high-temperature granite after water-cooling. *Rock Soil Mech* 42(06):1568–1578
- Junique T, Vázquez P, Géraud Y, Thomachot-Schneider C, Sidibé H (2021) Microstructural evolution of granitic stones exposed to different thermal regimes analysed by infrared thermography. *Eng Geol* 286:106057. <https://doi.org/10.1016/j.enggeo.2021.106057>
- Kang FC, Li YC, Tang CA (2021) Grain size heterogeneity controls strengthening to weakening of granite over high-temperature treatment. *Int J Rock Mech Min* 145:104848. <https://doi.org/10.1016/j.ijrmmms.2021.104848>
- Kim K, Kemeny J, Nickerson M (2014) Effect of rapid thermal cooling on mechanical rock properties. *Rock Mech Rock Eng* 47(6):2005–2019. <https://doi.org/10.1007/s00603-013-0523-3>
- Kumari WGP et al (2018a) Hydraulic fracturing under high temperature and pressure conditions with micro ct applications: geothermal energy from hot dry rocks. *Fuel* 230:138–154. <https://doi.org/10.1016/j.fuel.2018.05.040>
- Kumari WGP, Ranjith PG, Perera MSA, Chen BK (2018b) Experimental investigation of quenching effect on mechanical, microstructural and flow characteristics of reservoir rocks: thermal stimulation method for geothermal energy extraction. *J Pet Sci Eng* 162:419–433. <https://doi.org/10.1016/j.petrol.2017.12.033>
- Liu S, Xu J (2015) An experimental study on the physico-mechanical properties of two post-high-temperature rocks. *Eng Geol* 185:63–70. <https://doi.org/10.1016/j.enggeo.2014.11.013>
- Meredith PG, Atkinson BK (1985) Fracture-toughness and sub-critical crack-growth during high-temperature tensile deformation of Westerly granite and Black gabbro. *Phys Earth Planet Inter* 39(1):33–51. [https://doi.org/10.1016/0031-9201\(85\)90113-X](https://doi.org/10.1016/0031-9201(85)90113-X)
- Nasseri MHB, Schubnel A, Young RP (2007) Coupled evolutions of fracture toughness and elastic wave velocities at high crack density in thermally treated westerly granite. *Int J Rock Mech Min* 44(4):601–616. <https://doi.org/10.1016/j.ijrmmms.2006.09.008>
- Nasseri MHB, Schubnel A, Benson PM, Young RP (2009) Common evolution of mechanical and transport properties in thermally cracked westerly granite at elevated hydrostatic pressure. *Pure Appl Geophys* 166(5–7):927–948. <https://doi.org/10.1007/s00024-009-0485-2>
- Ohno I (1995) Temperature-variation of elastic properties of alpha-quartz up to the alpha-beta transition. *J Phys Earth* 43(2):157–169. <https://doi.org/10.4294/jpe1952.43.157>
- Ohno K, Ohtsu M (2010) Crack classification in concrete based on acoustic emission. *Constr Build Mater* 24(12):2339–2346. <https://doi.org/10.1016/j.conbuildmat.2010.05.004>
- Pathegama GR, Jian Z, Minghe J, Radhika VSDS, Tharaka DR, Adheesha KMSB (2017) 简评深部采矿的机遇与挑战. *Engineering-Prac* 3(04):250–261
- Shao SS, Ranjith PG, Wasantha PLP, Chen BK (2015) Experimental and numerical studies on the mechanical behaviour of Australian strathbogie granite at high temperatures: an application to geothermal energy. *Geothermics* 54:96–108. <https://doi.org/10.1016/j.geothermics.2014.11.005>
- Shen YJ, Hao JS, Hou X, Yuan JQ, Bai ZP (2021a) Crack propagation in high-temperature granite after cooling shock: experiment and numerical simulation. *Bull Eng Geol Environ* 80(7):5831–5844. <https://doi.org/10.1007/s10064-021-02259-6>
- Shen YJ, Yuan JQ, Hou X, Hao JS, Bai ZP, Li T (2021b) The strength changes and failure modes of high-temperature granite subjected to cooling shocks. *Geomech Geophys Geo-Energy Geo-Resour.* <https://doi.org/10.1007/s40948-020-00214-5>
- Shu B, Zhu R, Elsworth D, Dick J, Liu S, Tan J, Zhang S (2020) Effect of temperature and confining pressure on the evolution of hydraulic and heat transfer properties of geothermal fracture in granite. *Appl Energy* 272:115290. <https://doi.org/10.1016/j.apenergy.2020.115290>
- Smalley I, Marković SB (2019) Controls on the nature of loess particles and the formation of loess deposits. *Quatern Int* 502:160–164. <https://doi.org/10.1016/j.quaint.2017.08.021>
- Sun Q, Zhang WQ, Xue L, Zhang ZZ, Su TM (2015) Thermal damage pattern and thresholds of granite. *Environ Earth Sci* 74(3):2341–2349. <https://doi.org/10.1007/s12665-015-4234-9>
- Tian H, Zhu Z, Ranjith PG, Jiang G, Dou B (2021) Experimental investigation of drillability indices of thermal granite after water-cooling treatment. *Nat Resour Res* 30(6):4621–4640. <https://doi.org/10.1007/s11053-021-09926-1>
- Watanabe N et al (2020) Stabilizing and enhancing permeability for sustainable and profitable energy extraction from super-hot geothermal environments. *Appl Energy* 260:114306. <https://doi.org/10.1016/j.apenergy.2019.114306>
- Wu X et al (2022a) P-wave evolution and thermal conductivity characteristics in granite under different thermal treatment. *Chin J Rock Mech Eng.* <https://doi.org/10.13722/j.cnki.jrme.2021.0532>
- Wu Y, Peng K, Zou Q, Long K, Wang Y (2022b) Tensile properties and damage evolution laws of granite after high- and low-temperature cycles. *Nat Resour Res* 31(3):1289–1306. <https://doi.org/10.1007/s11053-022-10025-y>
- Xie H, Ju Y, Li L (2005) Criteria for strength and structural failure of rocks based on energy dissipation and energy release principles. *Chin J Rock Mech Eng* 17:3003–3010
- Yang SQ, Ranjith PG, Jing HW, Tian WL, Ju Y (2017) An experimental investigation on thermal damage and failure mechanical behavior of granite after exposure to different high temperature treatments. *Geothermics* 65:180–197. <https://doi.org/10.1016/j.geothermics.2016.09.008>
- Yin Q, Wu JY, Zhu C, Wang Q, Zhang Q, Jing HW, Xie JY (2021) The role of multiple heating and water cooling cycles on physical and mechanical responses of granite rocks. *Geomech Geophys Geo-Energy Geo-Resour.* <https://doi.org/10.1007/s40948-021-00267-0>

- Zhang Y, Zhao G (2020) A global review of deep geothermal energy exploration: from a view of rock mechanics and engineering. *Geomech Geophys Geo-Energy Geo-Resour* 6(1):4. <https://doi.org/10.1007/s40948-019-00126-z>
- Zhang F, Zhao JJ, Hu D, Skoczylas F, Shao JF (2018) Laboratory investigation on physical and mechanical properties of granite after heating and water-cooling treatment. *Rock Mech Rock Eng* 51(3):677–694. <https://doi.org/10.1007/s00603-017-1350-8>
- Zhu ZN, Kempka T, Ranjith PG, Tian H, Jiang GS, Dou B, Mei G (2021a) Changes in thermomechanical properties due to air and water cooling of hot dry granite rocks under unconfined compression. *Renew Energy* 170:562–573. <https://doi.org/10.1016/j.renene.2021.02.019>
- Zhu ZN, Ranjith PG, Tian H, Jiang GS, Dou B, Mei G (2021b) Relationships between p-wave velocity and mechanical properties of granite after exposure to different cyclic heating and water cooling treatments. *Renew Energy* 168:375–392. <https://doi.org/10.1016/j.renene.2020.12.048>

**Publisher's Note** Springer Nature remains neutral with regard to jurisdictional claims in published maps and institutional affiliations.